The effect of dimple shapes on friction of parallel surfaces

H Yu, H Deng, W Huang, and **X Wang***
College of Mechanical and Electrical Engineering, Nanjing University of Aeronautics and Astronautics, Nanjing, People's Republic of China

The manuscript was received on 20 October 2010 and was accepted after revision for publication on 15 March 2011.

DOI: 10.1177/1350650111406045

Abstract: In this study, the effect of different dimple shapes on the tribological performance of surface texture has been investigated. First, a numerical model was developed to study the effect of dimple shapes on hydrodynamic pressure generation. The selected dimple shapes include circle, square, and ellipse, and the flow direction of lubricant is perpendicular to the major axis of elliptical dimples or the sides of square dimples. The results showed that the dimple shape can be optimized for greater hydrodynamic pressure generation. Then, the reciprocating sliding tests were carried out under oil lubrication and face-contact conditions. Tests were conducted for rotational speeds in the range 50–500 r/min and test loads of 200 and 400 N. Surface texture patterns with different dimple shapes were used, the dimple shapes and orientations were the same as those used in the numerical model, and the dimple depth and dimple area ratio were varied under fixed dimple area conditions. The test results indicated that a better friction reduction effect compared with untextured specimens can be obtained by selecting a suitable dimple area ratio and dimple depth for each dimple shape. Comparing the friction reduction effect, the elliptical dimples showed the best performance, the square dimples showed the second best results, and the circular dimples performed worst. However, as the test load increased, the friction reduction effect of all dimple shapes decreased; moreover, the differences between the shapes became smaller.

Keywords: surface texture, dimple shape, friction coefficient, friction reduction

1 INTRODUCTION

Reducing friction and wear in mechanically interacting surfaces is important for increasing the working life of mechanical systems. Over the past decades, tribologists and lubrication engineers have been interested in surface modification for friction reduction and improved wear resistance. It is said that the surface is a novel material. Creating surfaces with controlled micro-geometry features is an effective method to improve tribological performance of sliding surfaces. In recent years, surface texturing has received a great deal of attention as a viable means to enhance the tribological performance of mechanical components; a large number of research studies have been carried out worldwide. The surface texture consisting of artificial micro-dimples or micro-grooves could benefit tribological pairs from boundary to hydrodynamic conditions [**1**–**3**]. Many studies [**4**–**6**] show that significant improvement in friction coefficient, wear resistance, and load-carrying capacity of tribological mechanical components can be obtained by the formation of reasonable surface textures on their surfaces. This improvement could be attributed mainly to the fact that the dimples on textured surfaces play a role as oil reservoirs, which can release the oil into the tribosystem in case of starved lubrication; the friction

**Corresponding author: College of Mechanical and Electrical Engineering, Nanjing University of Aeronautics and Astronautics, 29 Yudao Street, Nanjing 210016, People's Republic of China.*
email: xl_wang@nuaa.edu.cn

pair is therefore also sufficiently lubricated in boundary conditions [**7**]. At the same time, every dimple provides a pocket for wear particle embedment to prevent severe wear on the surfaces [**8**]. In addition, the dimple also serves as a micro-hydrodynamic bearing in cases of full or mixed lubrication to generate additional hydrodynamic pressure to increase the load-carrying capacity [**9**].

Recently, surface texturing has been successfully used in many applications to improve the tribological properties of sliding surfaces. For example, the surfaces of modern magnetic storage devices are commonly textured to reduce stiction during contact start–stop. Surface texturing is also considered as a means for overcoming adhesion and stiction in microelectromechanical systems (MEMS) devices. In 2004, laser surface texturing was successfully applied to mechanical seals, and both laboratory and field tests showed substantial friction reduction and up to threefold increase in seal life [**10**]. At the same time, various texturing techniques have been developed. These techniques include many traditional mechanical means such as milling and shot blasting [**11**]. A laser beam processing technique has also been widely applied [**10**, **12**], because it is efficient and convenient for metals. Reactive ion etching [**13**] and micro-electrolytic etching [**14**] show great potential for efficient texturing without undesirable effects; furthermore, it is easy to fabricate various dimple shapes on the surfaces.

Generating additional hydrodynamic pressure is usually considered as the most significant effect of surface texture under low-load and high-speed conditions, and has therefore attracted much more focused attention [**15**–**18**]. The surface textural parameters are the factors affecting hydrodynamic pressure generation. Etsion *et al.* [**15**] studied the effect of these parameters both in theory and by experiment. The authors indicated that the dimple depth to dimple diameter ratio is the most important factor. Recently, Raeymaekers *et al.* [**19**] and Yan *et al.* [**14**] also suggested that the dimple area ratio (ratio of dimples to surface areas) also greatly affects the tribological properties of the surface texture. Kligerman *et al.* [**20**] investigated the effect of texture design parameters on piston rings. They determined optimum values of texture depth and density for which a minimum of the friction force occurred. Wang *et al.* [**21**] studied the effect of dimple size on friction under line contact conditions, and the results indicated that the pattern with small dimple diameter showed a greater friction reduction effect than the pattern with the larger dimple diameter.

It is seen that so far, most studies are still focused on the effect of surface textural parameters such as dimple area ratio and size. There are only a few studies paying attention to the dimple shape effect [**22**–**24**]. Hence, this study will focus on the effect of the geometrical shapes of the surface texture on tribological performance. Three different surface textural shapes (circle, square, and ellipse) are selected in the following studies.

2 NUMERICAL ANALYSIS

In a previous study by the current authors [**25**], a numerical model was developed for the hydrodynamic lubrication region; however, the numerical model was based on just a single dimple. In order to improve calculation accuracy, taking into account the interaction between adjacent dimples and the effect on hydrodynamic pressure generation and reducing the calculation error caused by the boundary conditions, 3×3 dimple cells were selected as the computational domain in the current work, and a single dimple cell in the centre of the domain was studied. The same geometrical model as shown by Yu *et al.* [**25**] was selected. It is assumed that two surfaces are separated by a film thickness c, the lubricant is a Newtonian fluid, incompressible, and with a constant viscosity η. The relative speed between the two surfaces is U, unidirectional. Under the hydrodynamic lubrication condition, the fluid film pressure p is governed by the simplified Reynolds equation that can be expressed as

$$\frac{\partial}{\partial x}\left(h^3 \frac{\partial p}{\partial x}\right) + \frac{\partial}{\partial y}\left(h^3 \frac{\partial p}{\partial y}\right) = 6\eta U \frac{\partial h}{\partial x} \tag{1}$$

where h stands for the local film thickness, which can be calculated by the minimum film thickness c and the dimple depth h_p in the following form

$$h = \begin{cases} c + h_p & (x, y) \in \text{dimple area} \\ c & \text{else} \end{cases} \tag{2}$$

The fluid film pressure distribution can be obtained by solving the coupled equations (1) and (2). The ambient pressure was given at the border of the computational domain as a boundary condition. It is known that in the dimple area, the fluid film pressure increases in the film converging regions and decreases in the film diverging regions; however, the latter is bounded from below by cavitation. Thus, in the course of computation, the fluid film pressure will be replaced with cavitation pressure when it is lower than this level.

In the course of calculation, the surface textural parameters and other necessary conditions were provided as follows, and they are selected from the

following experimental settings as far as possible:

(a) area of a dimple $s = 31\,415\,\mu m^2$ (for the elliptical dimple, the major axis is 500 μm and the short axis 80 μm);
(b) dimple area ratio $r = 10.4$ per cent;
(c) dimple depth $h_p = 5\,\mu m$;
(d) ambient pressure $P_0 = 0.101\,325$ MPa;
(e) lubricant viscosity $\eta = 0.097\,33$ Pa s;
(f) the speed of the lower plate $U = 0.22$ m/s;
(g) minimum film thickness $c = 2\,\mu m$.

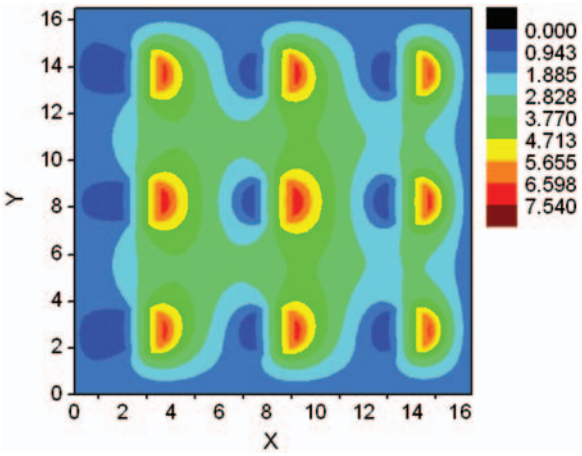

Fig. 1 Dimensionless fluid film pressure distribution in the computational domain

It should be noted that the dimples are arranged in a matrix pattern, and the flow direction of the lubricant is perpendicular to the major axis of elliptical dimples or the sides of square dimples.

Figure 1 shows the distribution of dimensionless fluid film pressure P generated by circular dimples in the computational domain. It can be seen that the pressure generated interacts between two adjacent dimples, and the larger dimensionless pressure can be found at the centre cell. Figure 2 shows the distributions of dimensionless fluid film pressure of the different dimple shapes from the centre cell of the computational domain. It is obvious that the dimple shape can affect fluid film pressure generation. By comparison, it is observed that the elliptical dimple has the largest fluid film pressure, the square dimple the second, and the circular dimple has the lowest fluid film pressure. The average values of centre-cell dimensionless pressure distribution are 3.57 for the elliptical dimple, 2.99 for the square dimple, and 2.72 for the circular dimple. Correspondingly, it can be

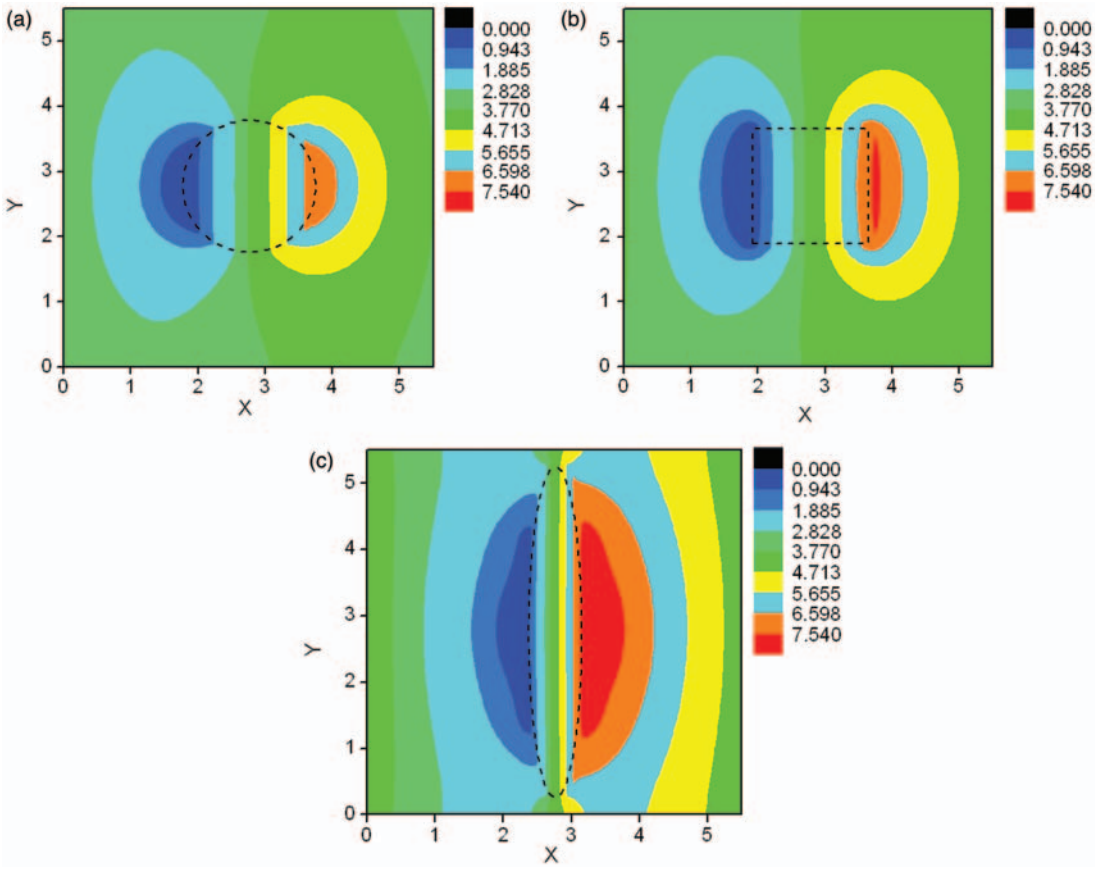

Fig. 2 Dimensionless fluid film pressure distribution of the centre cell in the computational domain: (a) circular dimple; (b) square dimple; and (c) elliptical dimple

speculated that when the load is fixed, larger film thickness can be obtained by the larger fluid film pressure generated by dimples, and asperity contact between two surfaces will be weakened more effectively for a lower friction. Hence, it can be concluded that the dimple shape can be optimized for optimum tribological performance.

3 EXPERIMENTAL PROCEDURE

The friction test was performed using a reciprocating friction test rig. As shown in Fig. 3(b), the upper specimen establishes face-to-face contacts with the lower specimen under the normal load. Both upper and lower specimens were cut from a commercial cylinder liner of a combustion engine made of boron–copper alloy cast iron. The Brinell hardness of boron–copper alloy cast iron is about *HB* 240–290, and the atomic composition of the material is summarized in Table 1. Before surface texturing, all specimens were first milled to create a flat surface and then ground to obtain the final surface with striated roughness R_a 0.4–0.5 μm. After machining was finished, the flat surface dimension of the upper specimen was $20 \times 20\,\text{mm}^2$ and that of the lower specimen $30 \times 140\,\text{mm}^2$. The surface roughness plays a deterministic role in influencing the tribological performance of sliding surfaces. According to Wang *et al.* [**26**], transverse roughness (perpendicular sliding direction) generates a higher average film pressure than the longitudinal roughness based on the same mean film thickness. Therefore, the same ground directions on the surfaces of upper and lower specimens are selected in this work; in addition, the ground direction is parallel to the sliding direction, as displayed in Fig. 4, so that the effect of surface texture could be emphasized.

In order to study the effect of different dimple shapes on the tribological performance of sliding surfaces, the surfaces of the upper specimens were textured with circular, square, and elliptical dimples, respectively. The geometrical shapes and texture parameters used in this research are summarized in Table 2. All surface textural shapes have the same dimple area $31\,415\,\mu\text{m}^2$ but different dimple depths and area ratios. The sliding direction is perpendicular to the major axis of elliptical dimples or the sides of square dimples. An upper specimen without surface texturing was also used for comparison. The texturing method used in this study was photoelectrolytic etching: masking by photolithography followed by electrolytic etching. A photoresist was spin coated onto the surface at a rotational speed of 1000 r/min for 10 s and then accelerated to 3000 r/min for 40 s. The coated surface was then pre-baked at 90 °C for 20 min. Contact masks for the patterns to be fabricated on the surfaces were designed by conventional desktop publishing methods and then photo-reduced

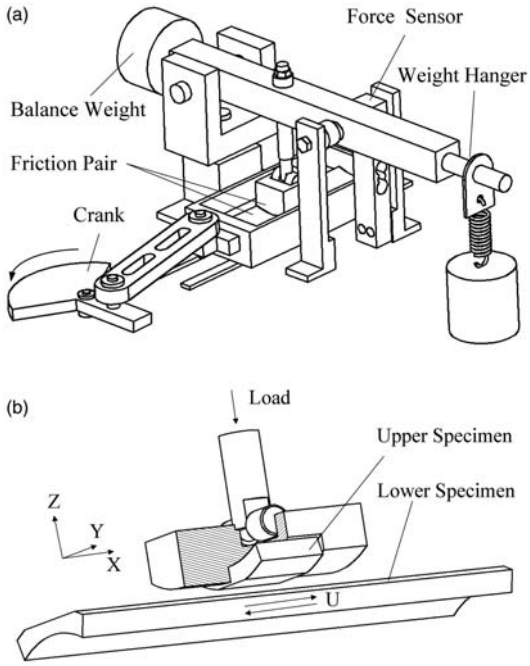

Fig. 3 Schematic diagram of reciprocating friction test rig: (a) test rig and (b) contact configuration of upper specimen and lower specimen

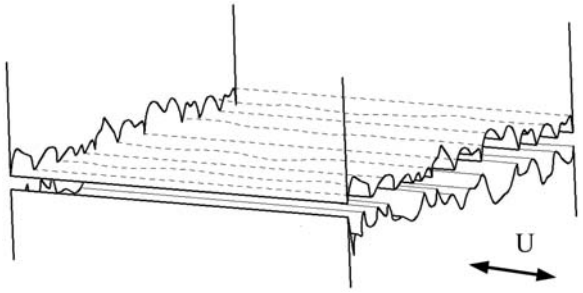

Fig. 4 Schematic diagram of ground direction on the surfaces of upper and lower specimens

Table 1 Atomic composition of material

Elements	C	Si	Mn	P	S	Cr	Cu	B	Fe
Contents (%)	2.8–3.4	2.0–2.6	0.5–1.0	≤0.3	≤0.1	0.2–0.4	0.5–1.0	0.04–0.07	Balance

Table 2 Geometrical shapes and surface texture parameters on upper specimens

	Pattern and sliding directions	Dimple size (μm)	Area of a dimple (μm^2)	Dimple depth (μm)	Dimple area ratio (%)
Circle	U	200 (diameter)	31 415	3–5 8–10 14–18	2.6 10.4 15.5 22.9
Square	U	177.24 (side length)	31 415	3–5 8–10 14–18	2.6 10.4 15.5 22.9
Ellipse	U	500/80 (axis length)	31 415	3–5 8–10 14–18	2.6 7.4 10.4

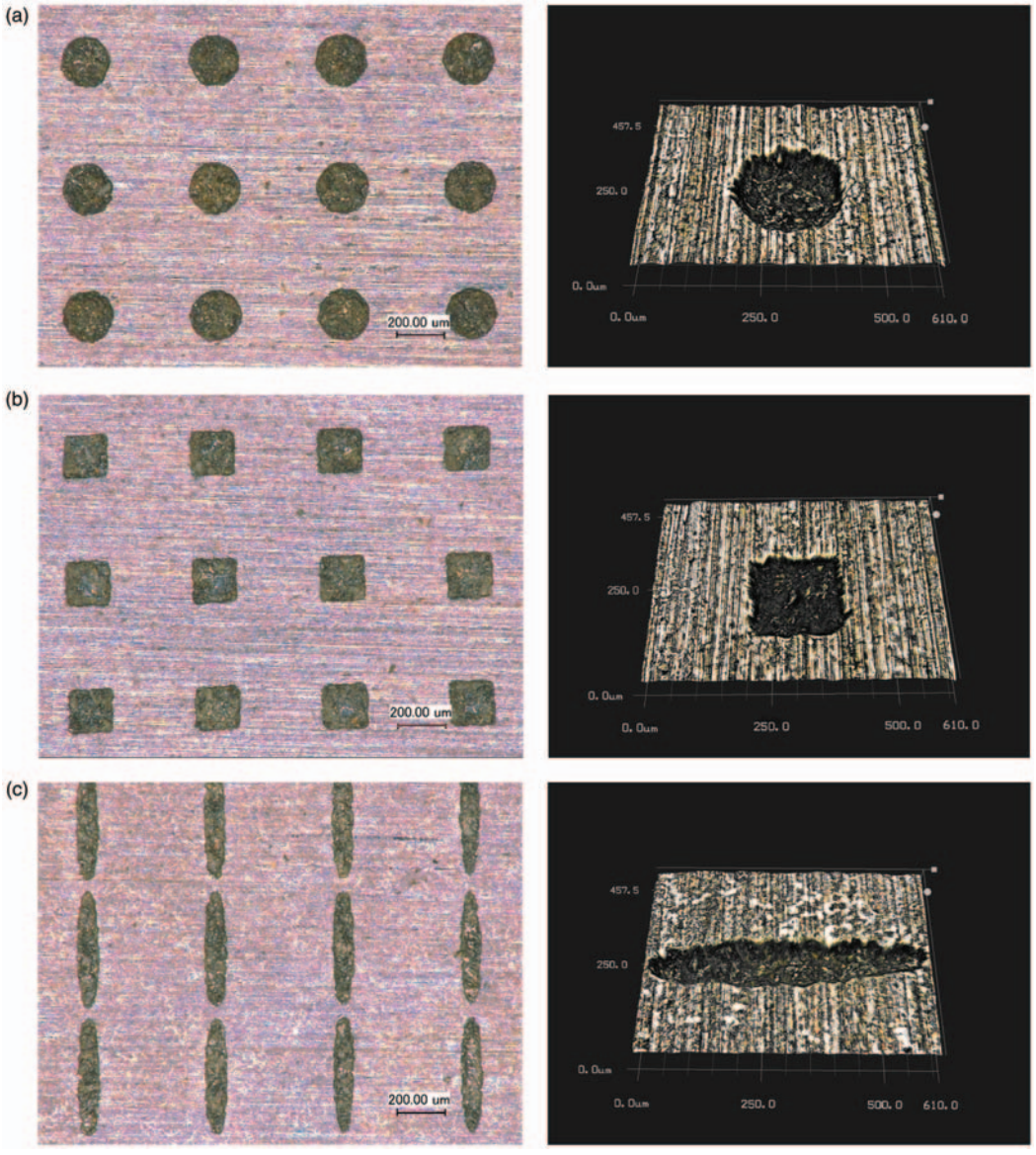

Fig. 5 Micrographs and 3D profiles of surface texture: (a) circular dimples with area ratio 10.4 per cent; (b) square dimples with area ratio 10.4 per cent; and (c) elliptical dimples with area ratio 10.4 per cent

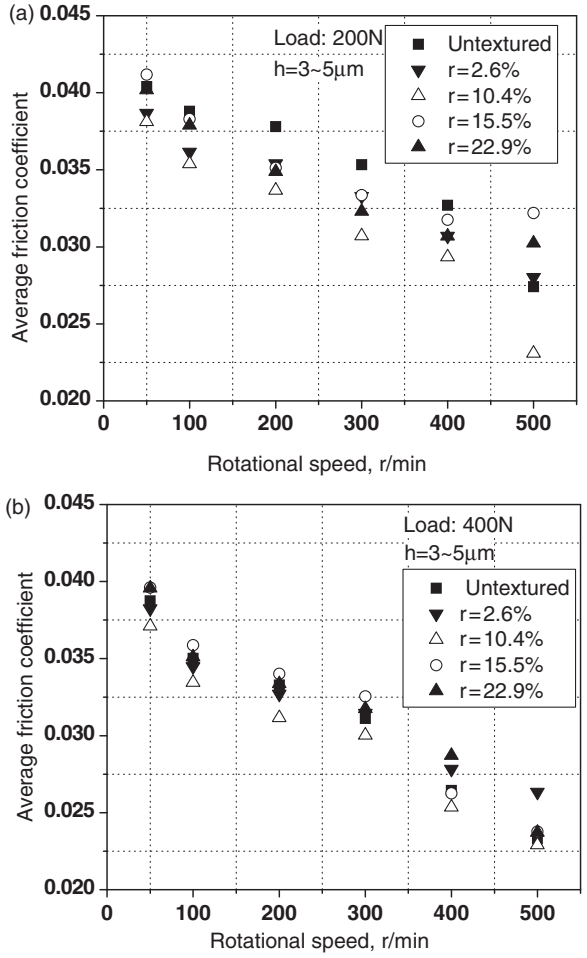

Fig. 6 The effect of the area ratio on the average friction coefficient for surfaces textured with circular dimples under different normal loads and rotational speed conditions

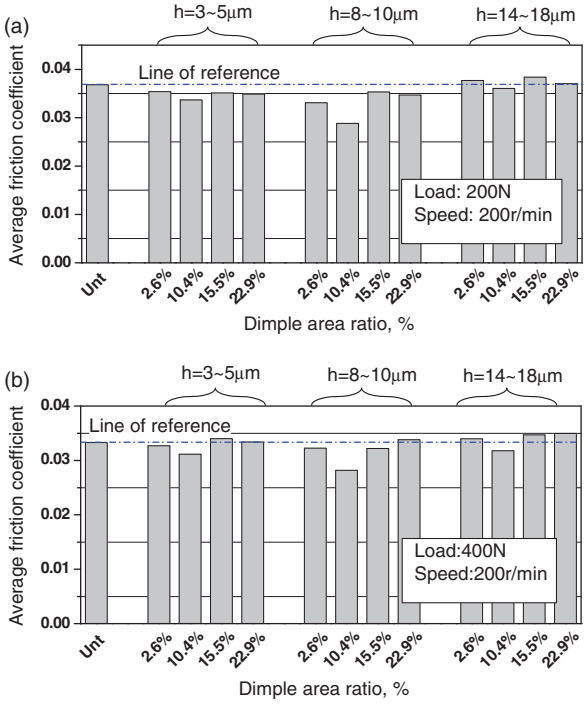

Fig. 7 The effect of the dimple depth on the average friction coefficient for surfaces textured with circular dimples under different normal loads

onto archive microfilm. The photoresist was exposed to ultraviolet light for 18 s, then developed in developing solution for 2 min, and then post-baked at 130 °C for 30 min. The surfaces were then etched in 10 per cent sodium nitrate solution, and the depths of the dimples were varied by controlling the etching time. Surface textures consisting of regularly repeating dimples with various geometries were produced. Figure 5 shows the micrographs and three-dimensional (3D) profile of three dimple patterns.

Reciprocating sliding tests were carried out under full lubrication conditions. The set-up of the system is shown schematically in Fig. 3(a). Sinusoidal linear motion of the lower specimens was generated by a crank mechanism, with a stroke length of 80 mm. A clamping fixture was used, as shown in Fig. 3(b), to avoid rotary motion of the upper specimens around the z-axis and to ensure that the upper specimens adapted to the lower specimens correctly. The normal load was applied by a dead weight of 200 to 400 N, which result in a mean contact pressure ranging from 0.5 to 1.0 MPa. The rotational speed of the crank was varied from 50 to 500 r/min, corresponding to a maximum sliding speed within a stroke of 0.21–2.1 m/s. A commercially available diesel engine oil CD 15 W-40 was used as the lubricant, which has a kinematic viscosity of 110.6 mm^2/s at 40 °C and 14.67 mm^2/s at 100 °C, and a viscosity index of 141. The lubricant was supplied at the beginning of each test; the volume supplied was 0.5 ml, a volume adequate for full lubrication. All the experiments were performed at room temperature, and the tests on each specimen were repeated twice. At each load, a running-in procedure was carried out for 15 min at 200 r/min, and then the friction force was recorded continuously by a data acquisition card and the friction coefficient calculated by a personal computer. In this paper, the average friction coefficient was used to evaluate the efficiency of the surface texture in terms of tribological performance. The average friction coefficient was calculated as the mean of absolute friction coefficients over 1000 reciprocating cycles for each group of test conditions.

4 RESULTS AND DISCUSSION

4.1 Effect of circular dimples

Figure 6 shows the effect of dimple area ratio on average friction coefficient for specimens textured

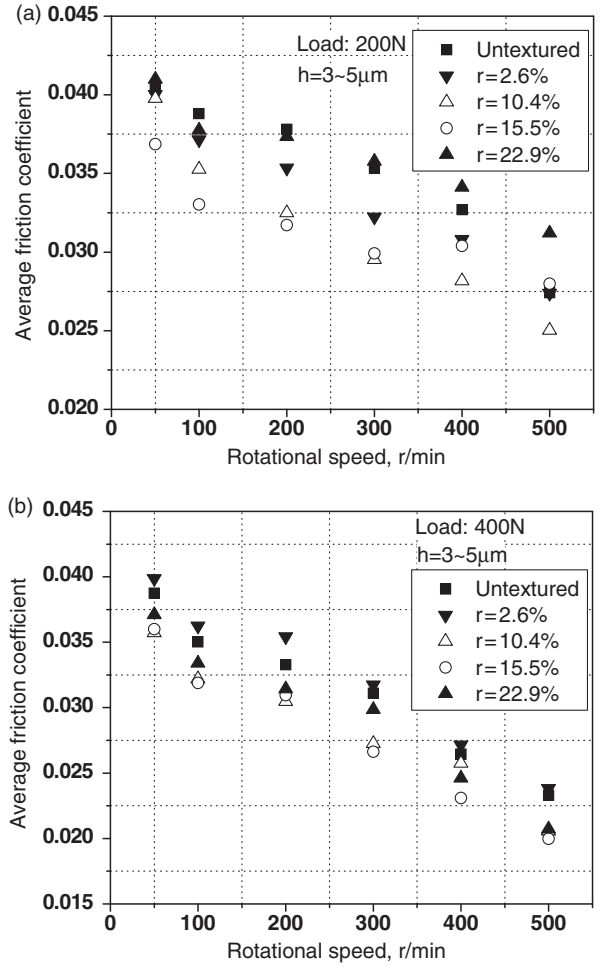

Fig. 8 The effect of the area ratio on the average friction coefficient for surfaces textured with square dimples under different normal loads and rotational speed conditions

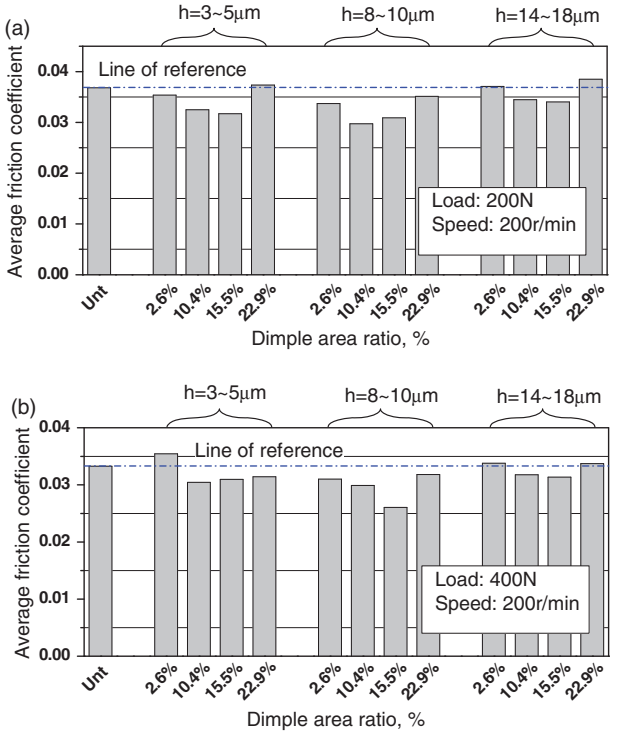

Fig. 9 The effect of the dimple depth on the average friction coefficient for surfaces textured with square dimples under different normal load

with circular dimples under different test load and rotational speed conditions. The dimple depth is around 3–5 μm, and the area ratio is varied in the range 2.6–22.9 per cent. Results are compared with an untextured surface. As can be seen, the average friction coefficient depended on the rotational speed. Also, this average friction coefficient decreased when the rotational speed increased, for all specimens. This indicates that a lubricant film has formed because of the existence of surface roughness, and the film formation is much easier at a higher rotational speed. On the other hand, the effect of the dimple area ratio on tribological performance seems to be substantial. Furthermore, the difference between different dimple area ratios decreased under a higher test load compared with that under a lower test load. In the case of low test load shown in Fig. 6(a), all the textured specimens showed lower average friction coefficients than the untextured specimen at rotational speeds from 100 to 400 r/min. The specimen with a dimple area ratio of 10.4 per cent showed the lowest value of average friction coefficient for all given rotational speeds, and showed a friction reduction of 15.7 per cent at the rotational speed of 500 r/min. Figure 6(b) shows the test results obtained at a relatively high test load of 400 N. The specimens with dimple area ratios of 15.5 per cent and 22.9 per cent had higher average friction coefficients compared with the untextured specimen. The dimple area ratio of 10.4 per cent still presented an average friction coefficient value smaller than that of the untextured specimen; however, the friction reduction was decreased. This implies that it is more difficult to reduce friction using surface texture under high test load than under a low test load.

The effect of dimple depth on the average friction coefficient is shown in Fig. 7 for the specimens textured with circular dimples under different test load conditions. The figure provides all the dimple area ratios and dimple depths used in this research. The experimental results in the figure were obtained at the rotational speed of 200 r/min, and it should be mentioned that similar results were also produced under other test rotational speed conditions. The line of reference indicates the results from the untextured specimen. As can be seen, the specimens with a dimple

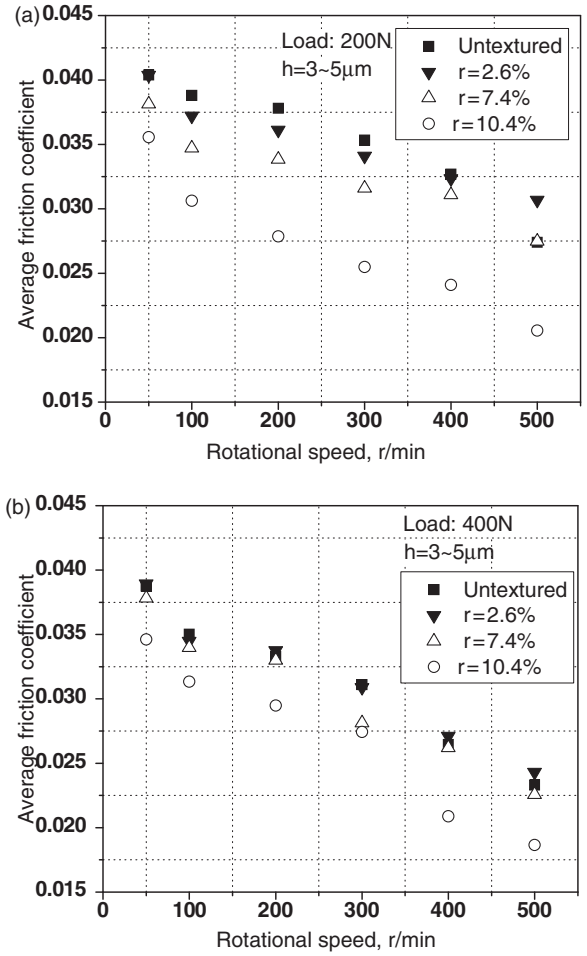

Fig. 10 The effect of the area ratio on the average friction coefficient for surfaces textured with elliptical dimples under different normal load and rotational speed conditions

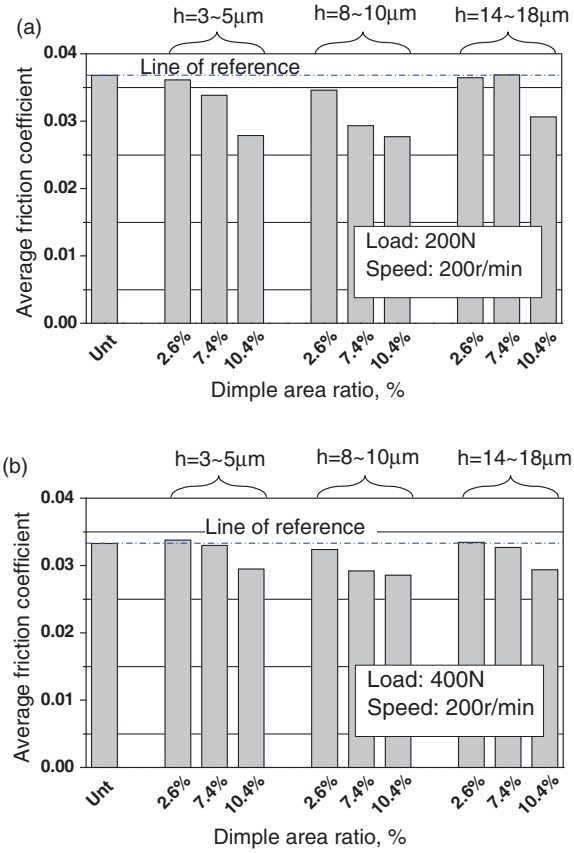

Fig. 11 The effect of the dimple depth on the average friction coefficient for surfaces textured with elliptical dimples under different normal load

area ratio of 10.4 per cent always give the most obvious friction reduction effect, although the dimple depth varies. The dimple depth has an effect on average friction coefficient. In the case of a low test load of 200 N, as shown in Fig. 7(a), it is clear that all the specimens with dimple depths of 3–5 and 8–10 μm show a better friction reduction effect compared with the untextured specimen; however, when the dimple depth is about 14–18 μm, only the specimen with a dimple area ratio of 10.4 per cent is better than the untextured specimen. When the test load increases to 400 N, all these effects of friction reduction become less marked. At both high and low test loads, an optimum dimple depth exists, which minimizes the average friction coefficient, and the optimum depth is around 8–10 μm.

4.2 Effect of square dimples

Figure 8 shows the effect of dimple area ratio on average friction coefficient for specimens textured with square dimples under different test load and rotational speed conditions. The variation of average friction coefficient with rotational speed shows a similar pattern to that in Fig. 6. Compared with the untextured specimen, dimple area ratios of 10.4 and 15.5 per cent both resulted in better friction reduction, and their reduction effectiveness is equivalent. In the case of a low test load of 200 N, as shown in Fig. 8(a), the maximum reduction rate of the average friction coefficient could be up to 16.4 per cent for the dimple area ratio of 15.5 per cent. However, this reduction rate decreases when the test load increases to 400 N.

Figure 9 shows the effect of the dimple depth on average friction coefficient for the specimens textured with square dimples under different test load conditions. It can be found that of all the dimple depths investigated in this research, the depth range of 8–10 μm gives the smallest average friction coefficient. Whether the test load is high or low, there is always an obvious friction reduction compared with untextured specimens.

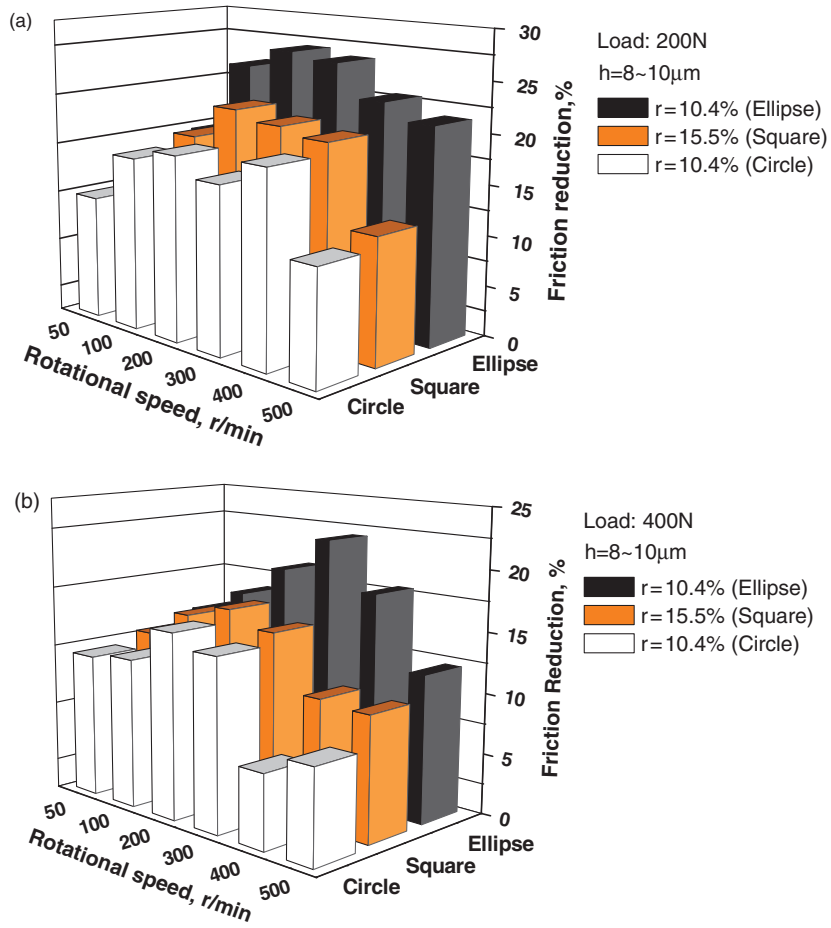

Fig. 12 The effect of dimple shape on friction reduction under different normal loads

4.3 Effect of elliptical dimples

Figure 10 shows the effect of dimple area ratio on average friction coefficient for specimens textured with elliptical dimples under different test load and rotational speed conditions. As can be seen from Fig. 10(a), compared with the untextured specimen, the specimens with the dimple area ratios of 7.4 per cent and 10.4 per cent both have an obvious friction reduction effect. In particular, the specimen with a dimple area ratio of 10.4 per cent resulted in the best friction reduction effect at all test rotational speeds, and the maximum reduction rate could be up to 26.3 per cent. On the other hand, the specimen with a dimple area ratio of 2.6 per cent had no better effect in terms of friction reduction than the untextured specimen. Figure 10(b) shows the results obtained at a relatively high test load of 400 N. Compared with the low test load condition of 200 N, the friction reduction effect described above became less marked.

Figure 11 shows the effect of the dimple depth on average friction coefficient for the specimens textured with elliptical dimples under different test load conditions. For both high and low test loads, almost all specimens with different dimple depths and dimple area ratios showed smaller average friction coefficient than those of untextured specimens. An optimum dimple depth of the range 8–10 μm was found, showing the best friction reduction.

According to the results shown above, it can be concluded that with the fixed dimple area, every dimple shape has an optimum dimple area ratio and an optimum dimple depth that give the best friction reduction effect.

4.4 Effect of dimple shapes

In order to further investigate the effect of dimple shapes on friction reduction, the optimum results from circular, square, and elliptical dimples were selected for comparison, as shown in Fig. 12. The graphs were drawn in the form of friction reduction rate, which is calculated by the quotient between f_Δ and f_{unt}, where f_Δ stands for the difference between average friction coefficient of untextured specimens

and that of textured specimens and f_{unt} the average friction coefficient of untextured specimens. It can easily be found that under both low and high test loads, the elliptical dimples have the best friction reduction effect, followed by the square dimples, and finally the circular dimples. The reason for this phenomenon might be that the elliptical dimples have the largest converging wedge of all the dimple shapes used in the research, and this larger converging wedge makes it easier to generate a lubricant film between two surfaces to prevent asperity contact. In addition, it can also be seen that the difference of friction reduction effect between square dimples and circular dimples is not marked. This might be due to the fact that their dimple sizes and the dimple shapes are similar when the dimple area is the same, so that their effects on the lubricant film generation are close to equal. In addition, when comparing Fig. 12(a) with Fig. 12(b), it can also be seen that as the test load increases, the friction reduction effect of all dimple shapes decreases; moreover, the differences between dimple shapes become smaller.

5 CONCLUSIONS

A numerical model was used to investigate the effect of different dimple shapes on hydrodynamic pressure generation between two parallel sliding surfaces. The selected dimple shapes include circle, square, and ellipse. The reciprocating sliding tests were then carried out to evaluate the tribological performance of specimens textured with different dimple shapes. The findings are summarized as follows.

1. The elliptical dimple generates the largest hydrodynamic pressure of the three dimple shapes, when the dimple area, area ratio, and dimple depth are the same.
2. With a fixed single dimple area, the smallest average friction coefficient can be obtained by changing dimple area ratio and dimple depth for each dimple shape. This suggests that an optimum friction reduction effect compared with the untextured specimen can be achieved by selecting suitable dimple parameters. In this research, the optimum parameters are a dimple area ratio of 10.4 per cent and a dimple depth of 8–10 μm for circular dimples, 15.5 per cent and 8–10 μm for square dimples, and 10.4 per cent and 8–10 μm for elliptical dimples.
3. The friction reduction effect also depends to a great extent on the dimple shapes. Of the dimple shapes investigated in this research, elliptical dimples always showed the best results under different test load and rotational speed conditions; the square dimples peformed the second best, and the circular dimples showed the worst results. Also, these test results showed a good correlation with those obtained from the numerical model.

FUNDING

The authors acknowledge the support of the National Nature Science Foundation of China (NSFC) (No. 50675101), Funding of Jiangsu Innovation Program for Graduate Education (No. CX10B_093Z-05), and Funding for Outstanding Doctoral Dissertation in NUAA (No. BCXJ09-06) for their financial support.

REFERENCES

1 **Kovalchenko, A., Ajayi, O., Erdemir, A., Fenske, G.,** and **Etsion, I.** The effect of laser texturing of steel surfaces and speed-load parameters on the transition of lubrication regime from boundary to hydrodynamic. *Tribol. Trans.*, 2004, **47**(2), 299–307.
2 **Wang, Q. J.** and **Zhu, D.** Virtual texturing: modeling the performance of lubricated contacts of engineered surfaces. *Trans. ASME, J. Tribol.*, 2005, **127**(4), 722–728.
3 **Wang, X., Kato, K.,** and **Adachi, K.** The critical condition for the transition from HL to ML in water-lubricated SiC. *Tribol. Lett.*, 2004, **16**(4), 253–258.
4 **Wang, X., Kato, K., Adachi, K.,** and **Aizawa, K.** Loads carrying capacity map for the surface texture design of SiC thrust bearing sliding in water. *Tribol. Int.*, 2003, **36**(3), 189–197.
5 **Zum Gahr, K. H., Mathieu, M.,** and **Brylka, B.** Friction control by surface engineering of ceramic sliding pairs in water. *Wear*, 2007, **263**(7–12), 920–929.
6 **Li, J. L., Xiong, D. S., Dai, J. H., Huang, Z. J.,** and **Tyagi, R.** Effect of surface laser texture on friction properties of nickel-based composite. *Tribol. Int.*, 2010, **43**(5–6), 1193–1199.
7 **Pettersson, U.** and **Jacobson, S.** Influence of surface texture on boundary lubricated sliding contacts. *Tribol. Int.*, 2003, **36**(11), 857–864.
8 **Suh, N. P., Mosleh, M.,** and **Howard, P. S.** Control of friction. *Wear*, 1994, **175**(1-2), 151–158.
9 **Hamilton, D. B., Walowit, J. A.,** and **Allen, C. M.** A theory of lubrication by micro-irregularities. *J. Basic Eng.*, 1966, **88**(1), 177–185.
10 **Etsion, I.** State of the art in laser surface texturing. *Trans. ASME, J. Tribol.*, 2005, **127**, 248–253.
11 **Nakano, M., Korenaga, A., Korenaga, A., Miyake, K., Murakami, T., Ando, Y., Usami, H.,** and **Sasaki, S.** Applying micro-texture to cast iron surfaces to reduce the friction coefficient under lubricated conditions. *Tribol. Lett.*, 2007, **28**, 131–137.
12 **Voevodin, A. A.** and **Zabinski, J. S.** Laser surface texturing for adaptive solid lubrication. *Wear*, 2006, **261**(11–12), 1285–1292.

13 **Wang, X., Adachi, K., Otsuka, K.,** and **Kato, K.** Optimization of the surface texture for silicon carbide sliding in water. *Appl. Surf. Sci.*, 2006, **253**(3), 1282–1286.

14 **Yan, D., Qu, N., Li, H.,** and **Wang, X.** Significance of dimple parameters on the friction of sliding surfaces investigated by orthogonal experiments. *Tribol. Trans.*, 2010, **53**, 703–712.

15 **Etsion, I., Kligerman, Y.,** and **Halperin, G.** Analytical and experimental investigation of laser-textured mechanical seal faces. *Tribol. Trans.*, 1999, **42**(3), 511–516.

16 **de Kraker, A., van Ostayen, R. A. J., van Beek, A.,** and **Rixen, D. J.** A multiscale method modeling surface texture effects. *Trans. ASME, J. Tribol. Trans.*, 2007, **129**(2), 221–230.

17 **Brenner, G., Al Zoubi, A., Mukinovic, M., Schwarze, H.,** and **Swoboda, S.** Numerical simulation of surface roughness effects in laminar lubrication using the lattice-Boltzmann method. *Trans. ASME, J. Tribol.*, 2007, **129**(3), 603–610.

18 **Wang, X., Kato, K., Adachi, K.,** and **Aizawa, K.** The effect of laser texturing of SiC surface on the critical load for the transition of water lubrication mode from hydrodynamic to mixed. *Tribol. Int.*, 2001, **34**(10), 703–711.

19 **Raeymaekers, B., Etsion, I.,** and **Talke, F. E.** A model for the magnetic tape/guide interface with laser surface texturing. In Proceedings of the ASME/STLE International Joint Tribology Conference, 2008, pp. 669–671.

20 **Kligerman, Y., Etsion, I.,** and **Shinkarenko, A.** Improving tribological performance of piston rings by partial surface texturing. *J. Tribol.*, 2005, **127**, 632–638.

21 **Wang, X., Liu, W., Zhou, F.,** and **Zhu, D.** Preliminary investigation of the effect of dimple size on friction in line contacts. *Tribol. Int.*, 2009, **42**(7), 1118–1123.

22 **Siripuram, R. B.** and **Stephens, L. S.** Effect of deterministic asperity geometry on hydrodynamic lubrication. *J. Tribol.*, 2004, **126**(3), 527–534.

23 **Lu, X. B.** and **Khonsari, M. M.** An experimental investigation of dimple effect on the stribeck curve of journal bearings. *Tribol. Lett.*, 2007, **27**(2), 169–176.

24 **Galda, L., Pawlus, P.,** and **Sep, J.** Dimples shape and distribution effect on characteristics of Stribeck curve. *Tribol. Int.*, 2009, **42**(10), 1505–1512.

25 **Yu, H., Wang, X.,** and **Zhou, F.** Geometric shape effects of surface texture on the generation of hydrodynamic pressure between conformal contacting surfaces. *Tribol. Lett.*, 2010, **37**(2), 123–130.

26 **Wang, S., Hu, Y. Z., Wang, W. Z.,** and **Wang, H.** Effects of surface roughness on sliding friction in lubricated-point contacts: experimental and numerical studies. *Trans. ASME, J. Tribol.*, 2007, **129**, 809–817.

APPENDIX

Notation

c	minimum film thickness (μm)
f_{unt}	average friction coefficient of untextured specimens
f_{Δ}	the difference between average friction coefficient of untextured specimens and those of textured specimens
h	local film thickness (μm)
h_p	dimple depth (μm)
p	fluid film pressure (MPa)
P	dimensionless fluid film pressure (p/P_0)
P_0	ambient pressure (MPa)
r	dimple area ratio (%)
s	area of a dimple (μm^2)
U	the speed of the lower plate (m/s)
η	lubricant viscosity (Pa s)